Commissioning an EUV mask microscope for lithography generations reaching 8 nm

Kenneth A. Goldberg[a], Iacopo Mochi[a], Markus Benk[a], Arnaud P. Allezy[a], Michael R. Dickinson[a], Carl W. Cork[a], Daniel Zehm[a], James B. Macdougall[a], Erik Anderson[a], Farhad Salmassi[a], Weilun L. Chao[a], Vamsi K. Vytla[a], Eric M. Gullikson[a], Jason C. DePonte[a], M. S. Gideon Jones[a], Douglas Van Camp[a], Jeffrey F. Gamsby[a], William B. Ghiorso[a], Hanjing Huang[a], William Cork[a], Elizabeth Martin[a], Eric Van Every[b], Eric Acome[b], Veljko Milanovic[c], Rene Delano[a], Patrick P. Naulleau[a], and Senajith B. Rekawa[a]

[a]Center for X-Ray Optics, Lawrence Berkeley National Laboratory, Berkeley, CA 94720
[b]Advanced Design Consulting USA Inc., 126 Ridge Rd, Lansing NY 14882, USA
[c]Mirrorcle Technologies, Inc., 2700 Rydin Road, Unit F, Richmond, CA 94804

ABSTRACT

The SEMATECH High-NA Actinic Reticle review Project (SHARP) is a synchrotron-based, EUV-wavelength microscope, dedicated to photomask imaging, now being commissioned at Lawrence Berkeley National Laboratory. In terms of throughput, resolution, coherence control, stability and ease of use, SHARP represents a significant advance over its predecessor, the SEMATECH Berkeley Actinic Inspection Tool (AIT), which was decommissioned in September 2012. SHARP utilizes several advanced technologies to achieve its design goals: including the first Fourier-synthesis illuminator on a zoneplate microscope, EUV MEMS mirrors, and high-efficiency freestanding zoneplate lenses with numerical aperture values up to 0.625 (4×). In its first week of operation, SHARP demonstrated approximately 150 times higher light throughput than AIT and a spatial resolution down to 55-nm half-pitch with 0.42 4×NA (i.e. the smallest feature size on our test mask.) This paper describes the current status of the tool commissioning and the performance metrics available at this early stage.

Keywords: extreme ultraviolet lithography, EUV, microscope, actinic, mask, reticle, imaging, zoneplate

1. INTRODUCTION

We are now commissioning a new, synchrotron-based extreme ultraviolet (EUV, near 13.5-nm wavelength) microscope to support advanced photomask research for the semiconductor industry. The microscope will serve photolithography generations to the year 2020 and beyond, when printed feature sizes are expected to fall below 10 nm. Called *SHARP* (the SEMATECH High-NA Actinic Reticle review Project), the microscope is designed to emulate the optical properties of current and future EUV lithography tools, enabling the study of mask defects, pattern architectures, optical proximity correction, phase-shifting patterns, and more.[1] SHARP is the successor to the SEMATECH Berkeley Actinic Inspection Tool (AIT) which was decommissioned in September, 2012 after eight years of operation.

Owing to their highly wavelength-specific optical properties, the creation of production-quality EUV masks may come to rely upon dedicated EUV-wavelength mask-blank inspection and pattern-imaging tools. With commercial tools still months to years years from deployment, SHARP was created by an industry/government partnership to provide advanced research and development capabilities.

Although rooted in similar technologies, SHARP is designed to surpass the AIT in almost every performance metric. The AIT was the first EUV microscope to achieve diffraction-limited imaging with zoneplate lenses,[2] and the first to offer an array of user-selectable zoneplate lenses, with different optical properties. To accomplish its goals, SHARP utilizes several advanced short-wavelength optical elements and systems. SHARP is the first EUV microscope to combine lossless, customizable coherence control[1] with zoneplate-lens imaging; and, it is the first to use a dynamic, MEMS-based EUV mirror element. In SHARP nearly 30 times more lenses will be available, providing customized

configurations for a range of azimuthal angles of incidence at each available numerical aperture value, and some redundancy for the zoneplate parameters anticipated to be in the highest demand.

SHARP's streamlined, Fourier-synthesis illuminator converts the narrow-divergence synchrotron light into arbitrary angular illumination patterns. Arrays of high-efficiency zoneplate lenses enable the emulation of current and future EUV printing tools with 4× numerical aperture values up to 0.625, central ray angles up to 10°, and azimuthal rotation of the plane of incidence, within ±25°. An in-situ visible-light microscope with brightfield and darkfield illumination supports mask navigation. The angular distribution of the EUV illumination is measued by a low-magnification (1.7×), pupil-fill monitor microscope placed below the mask plane; when raised into the mask plane, the same system records the illuminator's beam position and profile. A two-axis angle-scanning stage provides sub-100-μrad deflection of the final mirror in the illuminator to enable uniformity control.

Ultimately, we seek to investigate masks and to emulate the properties other current and future inspection and printing tools. Whether EUV lithography moves toward higher mask-side NA values or higher magnifications to achieve pattern size reduction, SHARP is designed accommodate several generations of EUV mask research.

SHARP's ongoing commissioning began in January 2013. Optimization for high performance operation has not been completed, but improvements in performance (in particular flux and resolution) are already evident. The original plans and goals for SHARP were discussed previously.[3] SHARP's mechanical system has also been discussed separately.[1] Here we describe several of SHARP's key optical systems, and provide early performance data where available.

2. SYSTEM DESCRIPTION

The system specifications can be divided into the optics (illuminator, and imaging), and the mechanical systems required to support them. Achieving high signal-to-noise ratios depends on delivering the maximum possible light-flux into the small imaging region. To that end, SHARP's simplified design contains only essential optical elements. Optically, the system's goal is to deliver the maximum available power from the beamline to a small region of the mask, while re-shaping the angular spectrum for coherence control, and providing uniform illumination over the 10–30-μm region of interest. Mechanically, the central challenge is to achieve nm-scale stability between the mask and the objective lens during 1–5-second exposures, a level that is required for accurate pattern measurements.

2.1 The Source and Illuminator

The SHARP microscope is powered by a synchrotron bending-magnet beamline at LBNL's Advanced Light Source, with a monochromator that provides tunable wavelength and bandwidth. At its focus, the beamline delivers approximately 14 μW of EUV power in a bandwidth, $E/\Delta E = 1000$, focused to a spot size of approximately 250 μm with horizontal and vertical angular divergences of approximately 2 × 4 mrad, respectively. (See Fig. 1.) A four-jaw slit is placed 2 m upstream of focus to decrease the beam divergence for finer coherence control, when necessary. A second four-jaw slit, just upstream of the focus, blocks stray light and allows us to control the lateral size of the beamline's focus, and thus the size of the illumination spot on the mask. This latter property can be important for reducing undesirable scattered light in some imaging conditions and pattern types. The slits are undergoing final preparation and have not been installed, as of February 2013.

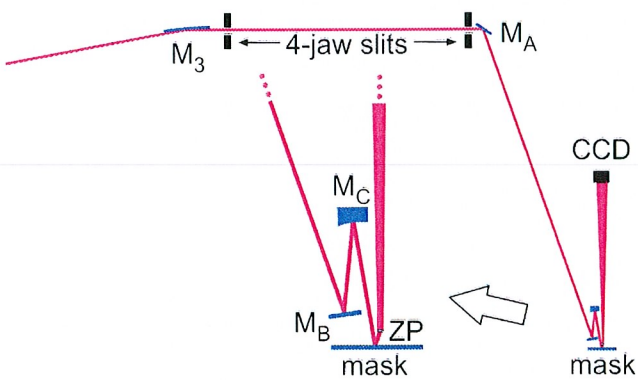

Figure 1. The beam path through the SHARP microscope. Inset detail shows a schematic of the M_B, M_C, the mask and the zoneplate (ZP) lens positions. The beamline's intermediate focus is on M_A.

2.1.1 Illumination Coherence Control. Shaping the angular pattern of the mask illumination gives lithographers additional control of the imaging performance, and enables pattern modulation at spatial scales below the coherent diffraction limit. SHARP is designed to emulate the partial coherence properties of arbitrary wafer-printing tools, using a lossless Fourier-domain illuminator[3,4] based on an efficient, three-mirror design. The illuminator converts the narrow-divergence, static beam from the synchrotron and dynamically fills arbitrary angular patterns during the exposures, while preserving flux. The illuminator has three mirrors we refer to as M_A, M_B and M_C. It produces a 10× demagnification of the beamline's intermediate focus and expand the angular range of light incident on the mask up to nearly 19° off-axis (encompassing central-ray angles of 6° to 10°, or more.)

The 10× demagnification reduces the beamline's 250-μm intermediate focus to a size that matches the microscope's typical field of view. Furthermore, the demagnification provides a 10x amplification of the range of ray angles leaving M_C, simplifying the design of the illuminator. The three mirrors are described here.

2.1.2 Dynamic EUV MEMS Mirror, M_A. The flat M_A mirror is a gimbal-less dual-axis, scanning MEMS device made from single-crystal silicon and integrated onto a dual inline "DIP24" package (see Fig. 2). Working with *Mirrorcle Technologies* of Richmond, California, we have developed a novel EUV-reflective version that can scan arbitrary angular pupil-fill patterns at speeds up to 2 kHz. The beamline's intermediate focus on M_A forms a virtual source for the illuminator that is imaged onto the mask surface by the elliptical M_C mirror.

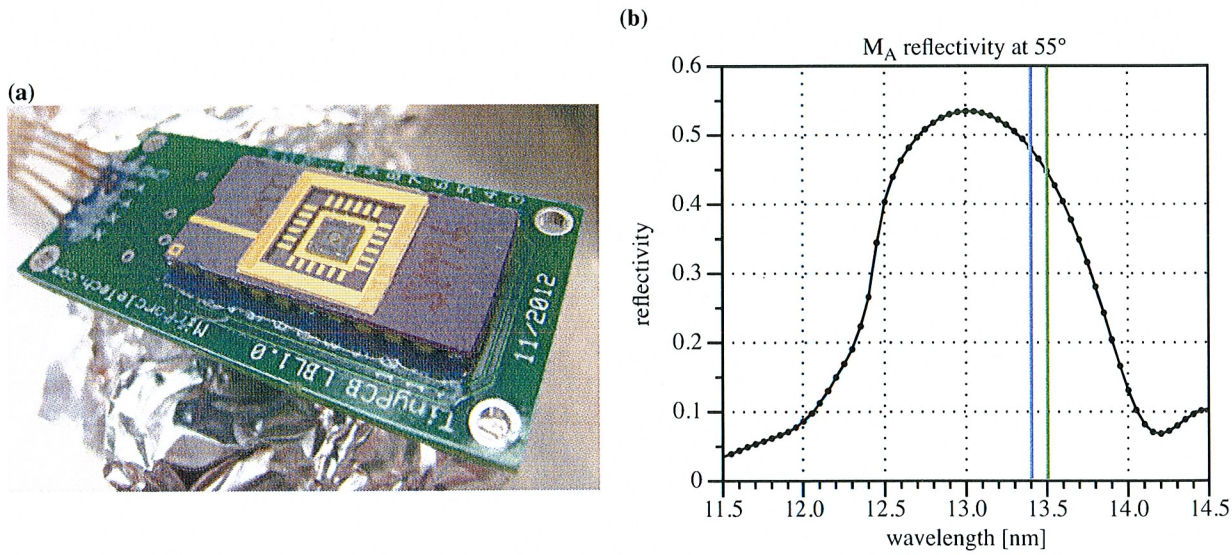

Figure 2. (a) The EUV MEMS mirror mounted on a circuit board. The mirror (at the center of the dip24 package) has 1-mm diameter. **(b)** Measured reflectivity vs. wavelength at the center of the M_A mirror, at the designed angle of operation, 55°.

Figure 2 contains a photograph of the M_A mirror, mounted for use, and the reflectivity of the device, versus wavelength, measured at the 55° operating angle of incidence. We deposited a multilayer coating with ten bi-layers to ensure an angular acceptance large enough to accommodate changes in the illumination angle during use, that range up to approximately ±1°. Figure 2b shows that the ML coating will have acceptable performance at 13.4–13.5-nm wavelength, but that improvements are possible. Details of the mirror preparation will be the subject of subsequent work.

2.1.3 M_B and M_C Mirrors. The flat M_B mirror folds the beam path upward into M_C. M_B has a narrow range of angles of incidence from 14.5 to 16.2°. Figure 3a shows the common M_B and M_C support structure mounted on an ex-situ pre-alignment system. The measured reflectivity of M_B at its central angle of incidence is shown in Fig. 3b.

The ellipsoidal mirror M_C (Fig. 3c) is the only curved mirror in the illuminator. It is designed for point-to-point imaging with 10× demagnification—every ray of light leaving the intermediate focus on M_A reaches a single point on the mask plane. *L-3 Tinsley* fabricated the M_C mirror to EUV surface-finish tolerances: 0.15-nm RMS, with slope errors below 25 μrad. M_C is wide in the transverse direction, enabling azimuthal rotation of the angle of incidence by ±25°. A conical

hole on the downstream side makes room for the upward-projected, diverging beam path from the zoneplate to the downward-facing EUV charge-coupled device (CCD) camera. The flat M_B is a folding mirror that directs the beam upward into M_C so the central angle of incidence on M_C is 10°. M_B keeps the incidence angles on M_C close to normal, simplifying M_C's multilayer coating.

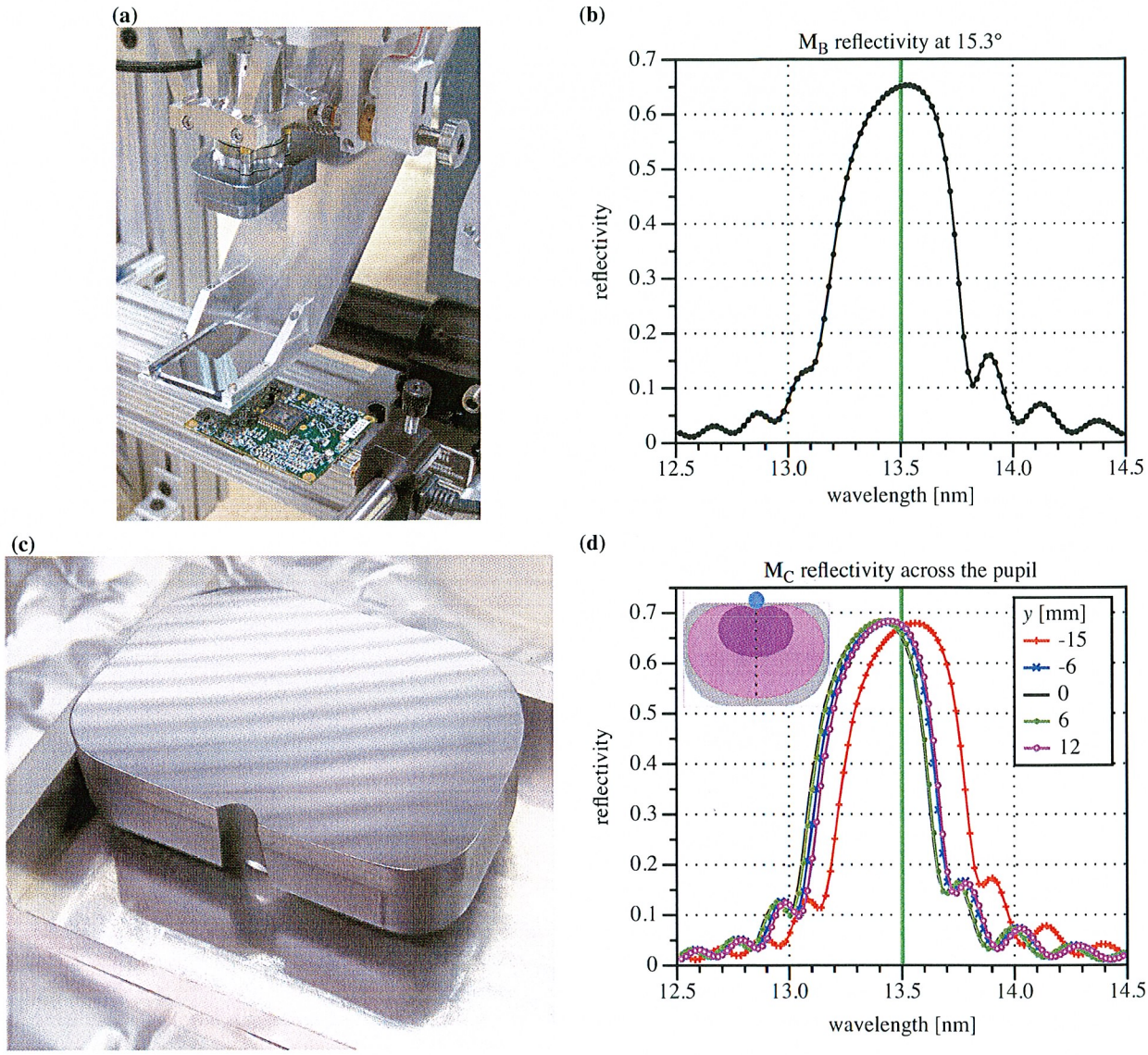

Figure 3. (a) The M_B (flat, lower left) and M_C (ellipse, upper right, downward-facing) mirrors mounted on their shared frame, configured for ex-situ pre-alignment, with a CCD camera in the plane normally occupied by a mask. **(b)** Measured reflectivity at the center of M_B, at the central angle of incidence. **(c)** The M_C mirror, before installation. It is approximately 48-mm wide. Here, the elliptical surface faces upward. The conical notch allows the upward-projected EUV image to pass close to the mirror. **(d)** M_C reflectometry was performed at a number of points across the narrow direction of the mirror, using the design angles of incidence. A subset of the data is shown.

The ellipsoidal shape of M_C gives it approximately 2 mm of concave surface sag, which combines with an angle-of-incidence gradient in the across the pupil to complicate the multilayer coating design. We developed a multilayer-coating strategy that accommodates the sag-dependent deposition rate in the coating chamber: a tilted mirror holder was created for the coating chamber to enable the multilayer *d*-spacing gradient to be achieved geometrically. Diamond-turned surrogate mirrors were used for iterative refinement of the coating prescription, before the final mirrors were coated.

Reflectometry performed across the M_C pupil, at the proper angles of incidence, shows high reflectivity at 13.5-nm wavelength (Fig. 3d).

The M_C mirror also acts as an illumination-uniformity scanner. Mounting M_C on a two-axis, tip-tilt stage with a peak frequency of 200 Hz enables us to steer the illumination focal point in a programmed pattern across the small field of view. The total angular range of the tip-tilt stage is limited to 50 μrad, small enough not to interfere with the 10–100-mrad angular illumination patterns created for coherence control.

2.2 Fresnel Zoneplate Objective Lenses

Fresnel zoneplate lenses (typically 100-μm diameter) project the image of the illuminated mask surface onto a 1-inch EUV CCD detector with 900× or higher magnification. The individual lenses are binary holograms of a single off-axis lens, created by electron-beam lithography.[5] The lenses operate in reflection, with focal lengths ranging from 266 to 750 μm depending on the required magnification. The incident beam illuminates a small region of the mask, and the lenses project the light directly upward to the CCD, a distance of approximately 450 mm above the mask surface.

For high-efficiency, the lenses are patterned in free-standing gold membranes, without the silicon-nitride membrane that supported similar zoneplates in the AIT. Furthermore, elliptically shaped open windows in the absorber membrane transmit the incident light without attenuation or the possibility of carbon-contamination build-up over time.

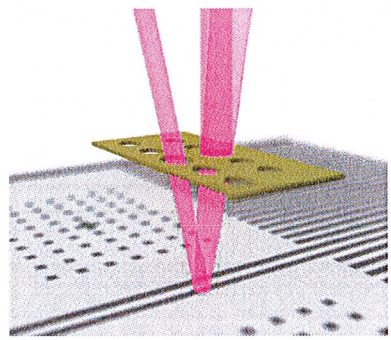

Figure 4. Cartoon of the reflective zoneplate geometry. The incident beam passes through an open window in the absorber membrane and illuminates the mask. The off-axis zoneplate projects the image directly upward to the CCD, while the undiffracted zeroth-order light propagates at a different angle.

Proper alignment of the lenses is critical to their diffraction-limited performance. Typical tilt-error tolerances are on the order of tenths of a degree, and become tighter as a function of NA. SHARP's zoneplates are mounted onto their holder using a kinematic ball-and-groove system (Figs. 5a and b), with the high-precision balls positioned glued into lithographically etched features on the zoneplate chip. Magnets embedded in the frame attract thin steel plates attached to the zoneplate chips creating a stable, firm clamping where the only contact is between the balls and the grooves.

(a) **(b)**

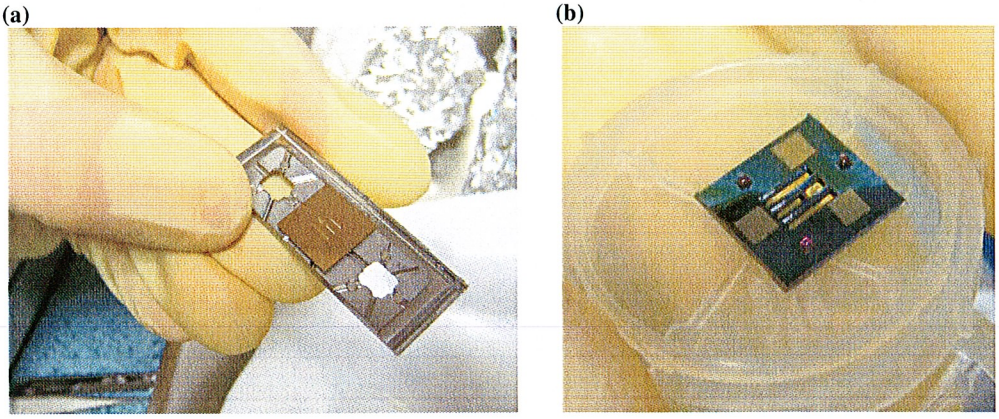

Figure 5. (a) a single zoneplate-array chip mounted onto a removable zoneplate holder. Both the chips and the holder rely on kinematic mounts for accurate, repeatable positioning. **(b)** The zoneplate array chip is 11-mm wide and contains four free-standing membranes.

The zoneplate holder and stages can accommodate three zoneplate-array chips. More than 70 different lenses are contained in each array. Each lens represents a specific 4×NA value (0.25, 0.33, 0.35, 0.42, 0.50, and 0.625 are available), and one of five azimuthal planes of incidence (-25°, -12.5°, 0°, 12.5, and 25°). The various azimuthal planes enable

SHARP to emulate the rotation of the incidence angles that occurs across the arc-shaped field of view in some printing tools. Figure 6a shows a detail with five lenses from the array. Figure 6b shows a close-up of the outer edge of one free-standing zoneplate. The narrow, stencil-like bridges provide strength to the structure at the cost of some throughput.

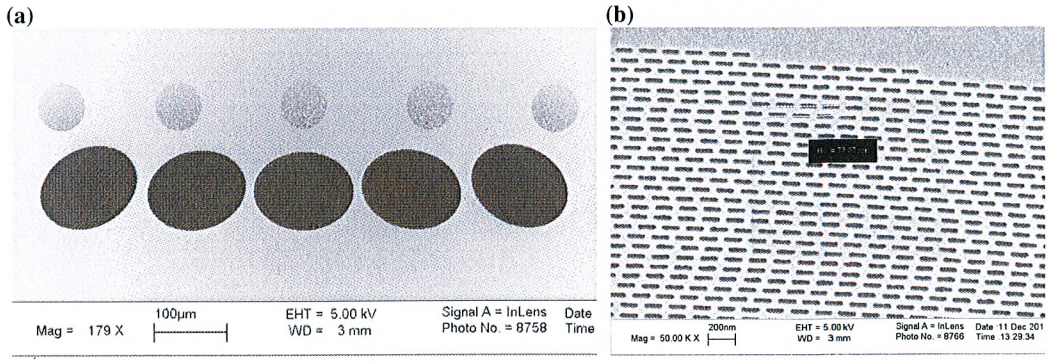

Figure 6. **(a)** SEM micrograph of a region of the zoneplate array containing five zoneplates and their associated windows. **(b)** The outer edge of one freestanding zoneplate, showing the stencil structure that gives it strength.

2.3 Pupil-Fill Monitor

Accurate control of the mask illumination requires feedback. We created a low-magnification in-vacuum microscope, called the *pupil-fill monitor* (PFM), to sample the incident light at different heights, monitoring the angular distribution and the beam profile in the mask plane. The PFM (shown in Fig. 7) consists of a 0.5-mm-thick yttrium-aluminum garnet (Ce:YAG) scintillator crystal to convert the EUV to visible light, with a 2× magnification, an achromatic lens pair, a visible-light board camera installed in a sealed box. The PFM is attached to the mask stage, allowing it to be positioned in the beam, and translated vertically, through the focus of the illuminator. The PFM has a field-of-view is 2.7 × 2.0 mm, and an expected resolution of 2.1 µm.

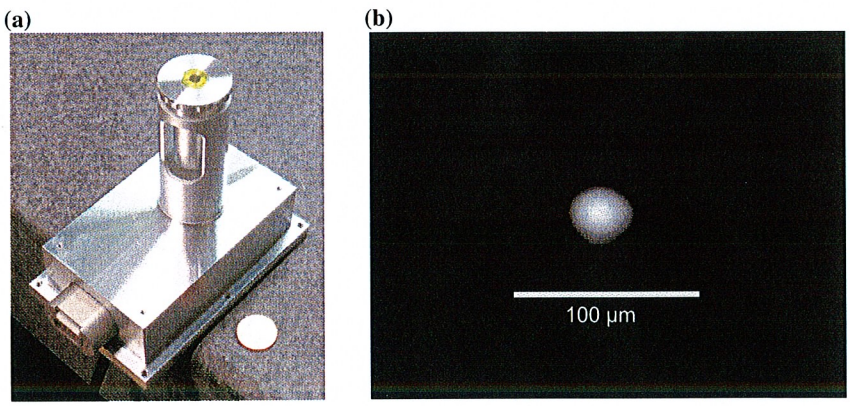

Figure 7. **(a)** The Pupil-Fill Monitor (PFM) camera before installation. A 2× microscope objective focuses the front surface of a YAG scintillator onto a visible-light board camera, in a sealed vessel. **(b)** An image detail of the focused EUV light from the illuminator, captured with the PFM.

2.4 Visible-light Mask Microscope

An in-situ visible-light microscope (VLM) with 2-µm resolution and a 1.33 × 1.00 mm field-of-view simplifies mask navigation, using pattern features and fiducial marks to improve position accuracy. The microscope is based on a long-working distance (34 mm), 0.14-NA 5× infinity-corrected microscope objective with an infinite conjugate, and a tube-lens relay optical system that projects the image to a CCD camera, positioned above the chamber lid. The optical components operate at air and are installed in a tube that projects downward into the vacuum chamber from above, with a vacuum window at the bottom. The VLM is equipped with a brightfield illumination system consisting of a diode, a collimating lens and beam splitter to make the illumination coaxial with the optics. A multi-mode darkfield illumination system is also being configured to use incoherent light (from in situ diodes) and/or coherent light from externally mounted lasers. We anticipate that the brightfield illumination will be most useful for patterned masks, and the darkfield for locating defects and fiducials on blank masks.

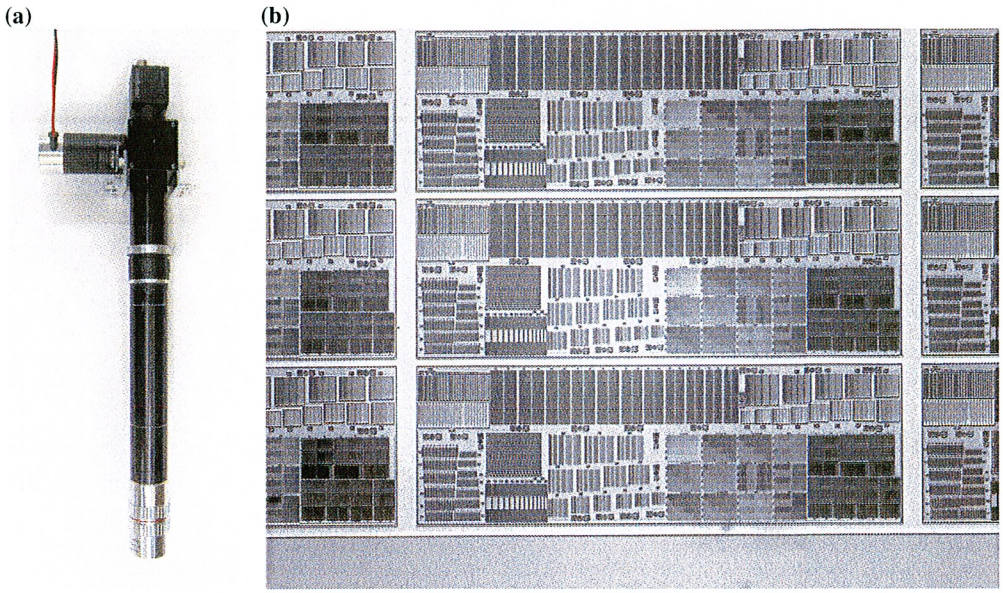

Figure 8. **(a)** The visible-light mask microscope (VLM), shown, projects downward into the chamber through a narrow tube to observe the mask surface. **(b)** An image of a mask test pattern field, recorded with the VLM. The image size is 1.33 × 1.00 mm.

3. MECHANICAL SYSTEM DESIGN

For high-magnification, nano-scale imaging, mechanical stability during multi-second exposures is the most important factor for success. Specifically, SHARP requires a sub-5-nm relative position of the mask and zoneplate during exposure. Thus the overall mechanical design is focused on the in-vacuum vibration isolation of the mask and zoneplate stages, achieved within a noisy experimental hall, in close proximity to pumps and other equipment.

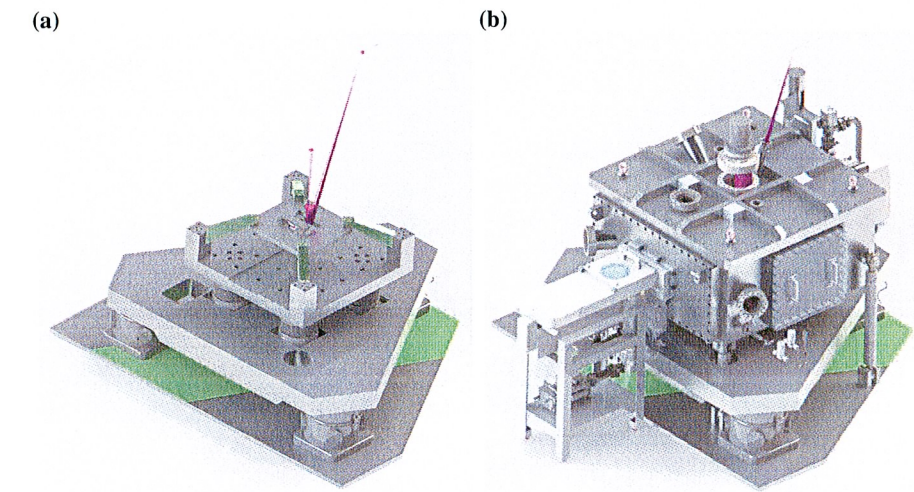

Figure 9. **(a)** CAD model of SHARP's vibration-isolation system: an isolated slab (triangular) supports an internal frame that contains the mask and zoneplate stages. **(b)** Model of the assembled system. The beam path is shown in magenta. The green stripe represents the location of a buried grade beam. The entire system will be enclosed in thermal/acoustic shielding (not shown).

3.1 Vibration Isolation

The design begins with a grouted, level floor plate that provides a common base for the chamber and the vibration-isolated platform. (See Fig. 9.) This plate bridges a buried grade beam that is a strong source of localized floor vibrations. Studies showed floor vibration levels of 10 nm integrated RMS displacement above 2 Hz. Three TMC STACIS® 2100 active piezoelectric vibration cancellation systems support a rigid, 4000-lb. steel plate in the space below the vacuum chamber. The system has an effective active resonant frequency of 0.5 Hz—the transmissibility at resonance is below 1.1 and it is designed to provide 90% isolation at 2 Hz. Inside the vacuum chamber, the unified mask and zoneplate stage support structure is attached to this aluminum plate through the bottom of the chamber using four pillars and flexible bellows. The chamber is independently supported by six struts tied to the floor plate.

3.2 Mask and Zoneplate Stage Support Frame

The mask and zoneplate array move independently, on two separate *xyz* stages. The *xy* mask stage travel exceeds 200 mm, enabling SHARP to reach every point on the mask surface with the zoneplate and the visible-light microscope. The *xyz* zoneplate stage hangs down from a shelf that is supported by a common frame with the mask stage. Both stages use magnetic position encoders to avoid stray-light in the chamber.

3.3 Mask Loading, Holding and Transfer

Mask loading occurs through a conventional robotic load-lock from *Transfer Engineering, Inc.* The mask is held onto the mask stage using a spring-loaded-tab system. This mask holder provides lateral position and angle repeatability of approximately 10 μm and 50 μrad. The gravitational sag of the mask supported in this manner induces an apparent tilt at the edges of the mask that is predicted to be below 16 μrad.

4. RESULTS

SHARP became operational in January 2013. Although optimization is still in progress, SHARP immediately demonstrated significantly higher power levels than AIT, with 153× higher flux reaching the CCD in one early measurement. To assess the power-level improvement, an experiment was conducted to match SHARP's operating conditions to that of AIT measurements performed in 2010: 0.35 4×NA zoneplate; 85-nm mask-half-pitch (hp), vertical line and space pattern; and the same small field of a test mask. Detail images are shown in Fig. 10 below.

4.1 Overall flux and image exposure time

To assess the power level, measurements were conducted using a calibrated photodiode on the mask stage, and using the EUV CCD camera itself. The photodiode reported 450 nW at 13.4-nm wavelength, in an energy bandwidth $\Delta E/E$ of 1/1450. As a point of reference, common exposure times in the AIT were 45 or 60 s, selected as an acceptable SNR for most measurements, with a slow but reasonable data-collection throughput. At that exposure time, most AIT images were recorded with less than 10% of the full dynamic-range capacity of the EUV CCD. Under matching operating conditions, SHARP demonstrated that with 2 s exposure times, the CCD recorded approximately 7× higher flux. The full-dynamic range of the CCD can be achieved with exposures less than 5 s.

We believe that even higher flux levels are possible with continued optimization of the system. The multilayer coating on the M_A mirror can be optimized for peak reflectivity at 13.5 nm. During the initial testing described here, mechanical constraints limited the mask stage *z* motion to 2.5 mm below the focus of the illuminator. The stages have since been modified to bring the mask into the illuminator focal plane where the flux will be higher and the coherence control can perform as designed. In addition, the zoneplates used in SHARP can operate with 50% larger energy bandwidths, as described in Section 2.2. We anticipate that the flux will be proportional to the operational bandwidth.

4.2 First Imaging data

A comparison of SHARP and AIT dense-line pattern measurements is shown in Fig. 10, including a 4×NA value of 0.35 for both AIT and SHARP (with 6° central ray angle), and 0.42 4×NA for SHARP (8° central ray angle). Mask hp values from 90 nm down to 55 nm were imaged. Smaller pattern sizes were not resolved on the mask. It is difficult to define the AIT partial coherence σ value precisely due to its unusual illumination properties, but estimates of its relatively high coherence, with σ of approximately 0.15, were effectively used for comparison to simulation.[6] In SHARP, the partial coherence used in the measurements shown here may be somewhat higher; quantitative analysis was not performed in the available time.

Comparison shows the relative performance of the mask imaging in these three states. The AIT data at 0.35 4×NA shows modulation with decreasing contrast down to 65-nm hp, the smallest feature size imaged on the AIT without tilting the illumination central ray off-axis. With somewhat higher σ, significantly higher signal, and improved stability, modulation in the SHARP data at 0.35 4×NA reaches to 65 nm, with observably higher contrast than the AIT. Below 65-nm, the 0.35 4×NA lens reached its spatial-frequency cutoff and no significant aerial image modulation was observable. Increasing the central ray angle to 8° and switching to a 0.42 4×NA lens, SHARP shows greater contrast in the same pattern pitch values, and modulation down to 55 nm, the mask's resolution limit.

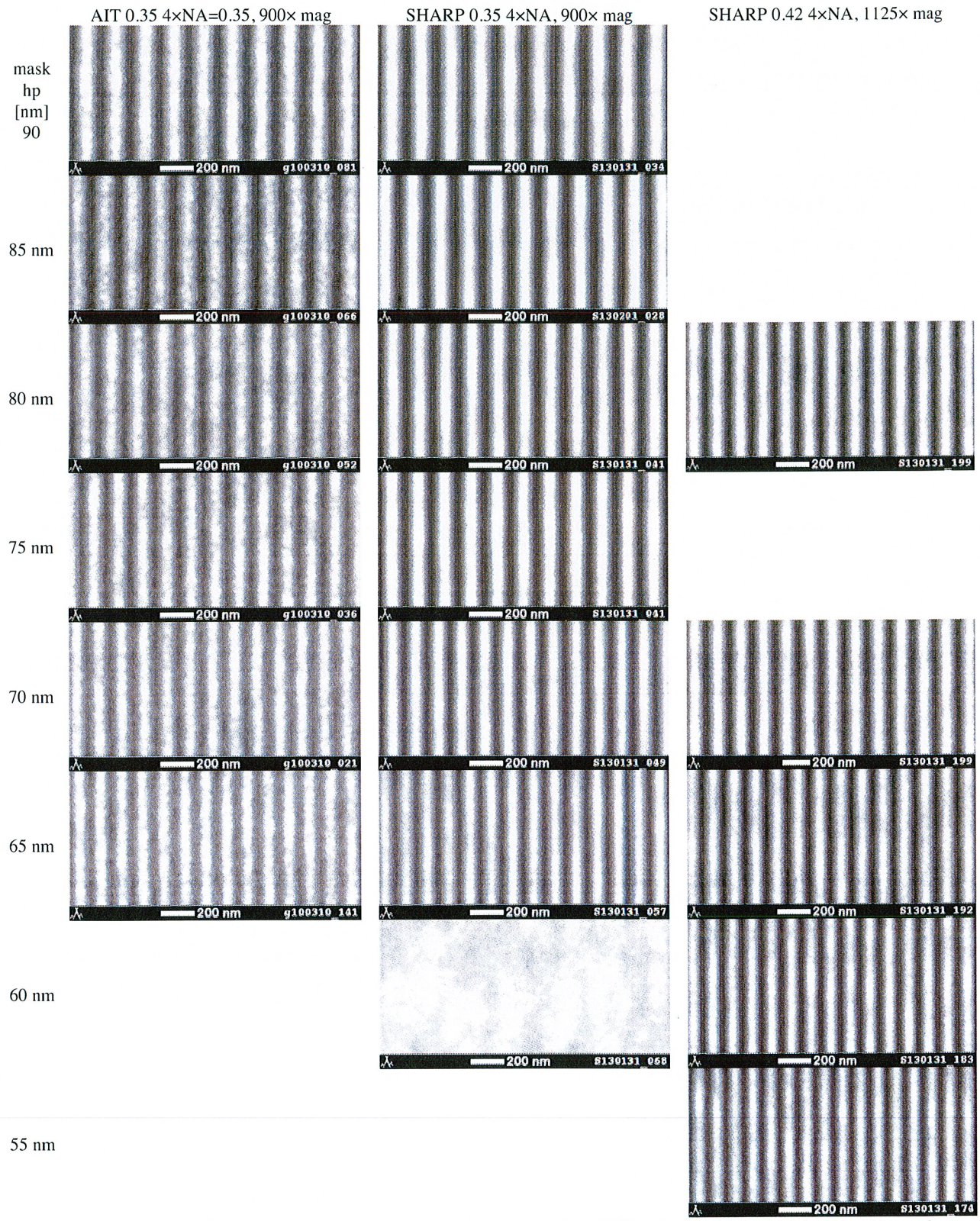

Figure 10. Side by side comparison of dense line pattern imaging in AIT (2010) and SHARP (2013). The NA values and magnifications are shown at the tops of each column.

The textured intensity pattern observable in the line patterns, especially in the AIT data, comes from a combination of speckle and shot noise. Multilayer phase roughness, coupled with optical aberrations, including defocus, gives rise to small-scale intensity variations, such as those observed here. We believe that the relative smoothness of the lines in the SHARP images arises from higher photon counts, and from the presence of some uncompensated astigmatism, occurring due to an imperfect alignment of the zoneplate lens. Further measurements will reduce astigmatism at the center of the field of view through alignment optimization.

5. CONCLUSION

The SHARP EUV-mask-imaging microscope became operational in January 2013 and demonstrated higher imaging resolution and photon flux than its predecessor, the AIT. While optimization of the illuminator is still in progress, early results show approximately 150x higher flux than the AIT in matched imaging conditions, on the same mask. With its continuously variable illumination angles, SHARP is able to use 4×NA values exceeding 0.35 at 6°, the AIT's limit. Mask images collected with 0.42 4×NA at 8° show resolution down to 55 nm, reaching the limit of our test mask. Higher resolution will be possible with SHARP's flexible illumination control, and zoneplate 4×NA values up to 0.625.

SHARP's design contains several innovations, including a lossless, Fourier-synthesis illuminator that is based on a high-performance EUV MEMS mirror and state of the art high-efficiency zoneplate lenses. An in-vacuum pupil-fill monitor provides quantitative assessment of the illumination pattern and focusing, and an in-situ visible-light microscope simplifies mask navigation.

Designed as a tool for advanced lithography research, SHARP's capabilities are aimed at both current and future generations of EUV lithography, whether they include higher mask-side NA values, or higher imaging demagnifications.

6. ACKNOWLEDGMENTS

We wish to acknowledge the guidance and direction of SEMATECH project leaders David Chan, Andy Ma, and Chihcheng Lin, the steadfast support of SEMATECH Bryan Rice, Stefan Wurm, and Frank Goodwin, and the SEMATECH member company leaders who have championed this project. The mask used in the high-resolution testing was supplied by Emily Gallagher and the IBM Mask House. This work was performed under the auspices of the U.S. Department of Energy by the University of California Lawrence Berkeley National Laboratory under management and operating contract DE-AC02-05CH11231. This work was funded by SEMATECH under Agreement No. LB08005006.

7. REFERENCES

[1] K. A. Goldberg, I. Mochi, M. P. Benk, A. P. Allezy, N. S. Smith, C. W. Cork, W. Cork, J. Macdougall, W. L. Chao, E. H. Anderson, P. P. Naulleau, E. Acome, E. Van Every, V. Milanovic, S. B. Rekawa, "Creating an EUV Mask Microscope for Lithography Generations Reaching 8 nm," *Precision Engineering and Mechatronics Supporting the Semiconductor Industry*, 4–7 (2012).

[2] I. Mochi, K. A. Goldberg, P. Naulleau, S. Huh, "Improving the performance of the Actinic Inspection Tool with an optimized alignment procedure," *SPIE* **7271**, 727123, (2009).

[3] K. A. Goldberg, I. Mochi, S. B. Rekawa, N. S. Smith, J. B. Macdougall, P. P. Naulleau, "An EUV Fresnel zoneplate mask-imaging microscope for lithography generations reaching 8 nm," *SPIE* **7969**, 79691O (2011).

[4] P. Naulleau, K. Goldberg, P. Batson, J. Bokor, P. Denham, and S. Rekawa, "A Fourier-synthesis custom-coherence illuminator for EUV microfield lithography," *Appl. Opt.* **42** (5), 820–26 (2003).

[5] K. A. Goldberg, P. Naulleau, I. Mochi, E. H. Anderson, S. B. Rekawa, C. D. Kemp, R. F. Gunion, H.-S. Han, S. Huh, "Actinic extreme ultraviolet mask inspection beyond 0.25 numerical aperture," *J. Vac. Sci. Technol. B* **26** (6), 2220–4 (2008).

[6] K. A. Goldberg, I. Mochi, P. P. Naulleau, H.-S. Han, S. Huh, "Benchmarking EUV mask inspection beyond 0.25 NA," *SPIE* **7122**, 71222E (2008).

DISCLAIMER

This document was prepared as an account of work sponsored by the United States Government. While this document is believed to contain correct information, neither the United States Government nor any agency thereof, nor The Regents of the University of California, nor any of their employees, makes any warranty, express or implied, or assumes any legal responsibility for the accuracy, completeness, or usefulness of any information, apparatus, product, or process disclosed, or represents that its use would not infringe privately owned rights. Reference herein to any specific commercial product, process, or service by its trade name, trademark, manufacturer, or otherwise, does not necessarily constitute or imply its endorsement, recommendation, or favoring by the United States Government or any agency thereof, or The Regents of the University of California. The views and opinions of authors expressed herein do not necessarily state or reflect those of the United States Government or any agency thereof or The Regents of the University of California.

This work was supported by the Director, Office of Science, of the U.S. Department of Energy under Contract No. DE-AC02-05CH11231.